Development of plasticity in vitrimers synthesized from a semi-crystalline polymer using injection molding

Laurent Farge, Rémi Spiegel, Stéphane André, Camille Noûs, Richard Lainé, Sandrine Hoppe

Development of Plasticity in Vitrimers Synthesized from a Semi-crystalline Polymer using Injection Molding

L. Farge[1*], R. Spiegel[1], S. André[1], C. Noûs[1,3], R. Lainé[2], S.Hoppe[2]

1 Université de Lorraine, CNRS, LEMTA, F-54000 Nancy, France

2 Université de Lorraine, CNRS, LRGP, F-54000 Nancy, France

3 Cogitamus Laboratory, F-75005 Paris, France.

*Corresponding author: laurent.farge@univ-lorraine.fr

Keywords

Vitrimers, Cross-linking, PBT, Mechanical properties

Abstract

The main objective of this work is to analyze finely the influence of cross-linking on the mechanical properties of PBT (Polybutylene Terephtalate)-based vitrimers. Tensile tests were carried out at four temperatures (80°C, 100°C, 130°C and 160°C) on a series of vitrimer specimens made by injection molding for which the cross-linker concentrations were changed by small increments of 0.25%, from 0% to 2%. The displacement and strain fields were measured on the specimen surfaces through 3 D DIC (Digital Image Correlation) in order to analyse the strain localization/delocalization phenomena that occur during the successive stages of the deformation process. In particular, we measured the yield strain ε_Y *(onset of strain localization), and the strain at neck stabilization* ε_{NS} *(beginning of the strain delocalization phase). When the degree of cross-linking increases, we observed two complementary effects leading to the decrease of the strain range during which plastic instability develops: Firstly* ε_Y *increases. Secondly, and this is the main cause of the plastic instability strain range reduction,* ε_{NS} *decreases. This latter effect results from the limitation in extensibility of the macromolecular network in the solid state caused by cross-linking. More specifically, cross-linking leads to two distinct modifications of the macromolecular network that both contribute to the reduction of its extensibility. The first is the decrease of the chain length between the network nodes. The second is the pre-orientation of the macromolecular network that occurs during injection molding in the case of vitrimers with high viscosities due to cross-linking. Eventually, when* $\varepsilon_Y \rightarrow \varepsilon_{NS}$*, the suppression of the yield point on the tensile curve was observed for the most cross-linked vitrimers. Furthermore, in the temperature range of investigation,* ε_{NS} *was found to be independent of temperature.*

Introduction

Semi-crystalline polymers deformed in tension at test temperatures between the glass transition and melting temperatures exhibit ductile behavior and can be deformed to large strains without breaking, typically greater than 300% (or true strain>1).[1-3]At the beginning of the deformation process, the strain is uniform along the specimen gauge length. Plastic instability leading to strain localization (necking) begins when the first Considère condition is met—i.e., at the yield point when the nominal stress reaches a maximum. Next, the nominal stress decreases before reaching a minimum as the strain in the neck increases much faster than in the other specimen parts. Neck is stabilized when the material in this region has hardened sufficiently to cause other regions of the specimen to deform instead. This "strain delocalization" phase is called "neck stabilization" or "neck propagation".[4-7] Without deformation field measurements but through a qualitative analysis of the characteristic tensile curves of different semi-crystalline polymers, Vincent has inferred indirectly that neck stabilization begins at the nominal stress minimum. This is the second Considère condition.[2]

At the microstructure level, strain hardening leading to neck stabilization is considered to be caused by the molecular network limitation in extensibility.[8-9] The nodes of this network consist initially of chain entanglements and connection points between adjacent crystals linked by tie molecules.[10] At large strain levels, when neck stabilization occurs, the lamellae are disintegrated into small fragments and the deformation process depends chiefly on the entangled amorphous network characteristics.[11-12] The higher the network node density, the lower the strain level at which neck stabilization occurs. Furthermore, if a polymer has a certain degree of orientation before deformation, the remaining extensibility of the macromolecular network in the solid state will be reduced and the strain at neck stabilization will be lowered.[13-15]

In addition to the just described scheme, some semi-crystalline polymers like polyethylene may also exhibit a second yield point,[7,16-17] but this was never observed for PBT (Polybutylene Terephtalate), the semi-crystalline polymer studied in this work.

Vitrimers are a new family of polymers that was invented in the beginning of the 2010s by Leibler and collaborators.[18-21] They are synthesized by "introducing" exchangeable chemical cross-links between the chains of a precursor polymer. The mechanism of cross-link migration is thermally activated. For the vitrimers with thermoplastic precursors, when the exchange reaction speed is low in the solid state, "vitrimerization" leads to an enhancement of the dimensional stability thanks to cross-linking. By contrast, in the molten state, the speed of exchange reactions increases and in spite of the presence of cross-links between the chains, the material may remain readily formable.

In 2017, Demongeot et al. developed an experimental protocol to "vitrimerize" PBT.[22] In addition to this semi-crystalline polymer, the reactive mixture contains a diepoxid, the cross-linker, and Zn(II), the catalyst of the transesterification reaction that causes cross-linking and bond exchange. DSC (Differential Scanning Calorimetry) measurements have shown that the vitrimer glass transition and melting temperatures are nearly the same as those of their PBT precursor.[22-23] Only a slight decrease of the crystallinity degree was observed for the vitrimers relatively to the pristine PBT. The cross-linking is assumed to take place in the inter-crystalline amorphous phase. A very schematic representation of the specific microstructure of PBT-based vitrimers is shown in Figure S1.

In a recent study, we reproduced the Demongeot et al. experimental protocol and we showed that the deformation process differs greatly between the pristine PBT and vitrimers obtained with cross-linker concentrations of 1% and 2%.[23] We found that the vitrimer nominal stress curves increase monotonically, which means that the yield point was suppressed for these materials. However, the physical mechanisms leading to the suppression of the necking behavior in vitrimers were not analysed in details. This is the purpose of the present paper. To this end, we carried out tensile experiments on the pristine PBT and on a series of PBT-based vitrimers for which the diepoxide cross-linker concentrations have been varied in small increments (≈0.25 wt%) from 0% to 2%. This makes it possible to study in a quasi-continuum way the evolution of the mechanical properties between two extreme cases, namely:

1) that of the pristine PBT, which is in line with the semi-crystalline polymers classical scheme recalled above,
2) that of vitrimers with high cross-linker concentrations that exhibit no yield point on the nominal stress curve.

In order to analyse specifically the strain localization/delocalization phenomena that occur during the deformation process, 3D Digital Image Correlation (3D DIC) measurements were performed to obtain the strain and the displacement fields at the specimen surfaces both in the Eulerian and Lagrangian descriptions. From a more general perspective, our work brings new insight of how the cross-linking of the amorphous phase of semi-crystalline polymers can fundamentally modify the development of plasticity in these materials, in particular when they are made by injection molding.

1 Experimental section

1.1 Vitrimer production

Along with the PBT precursor, the chemical reagents that were introduced in the µcompounder (DSM Xplore) at 270°C are the diepoxide—the cross-linker—the Zn(II) catalyst and an anti-oxidant. The PBT

precursor was provided by DuPont in pellet form (Material reference: CRASTIN FGS600F40). The diepoxide was the bisphenol-A epichlorhydrin resin DER332 produced by Olin epoxy. It is further referenced by the common abbreviation "DGEBA". The Zn(II) acetylacetonate hydrate was provided by Sigma Aldrich, as well as the anti-oxidant (Irganox 1010). In short, the reaction between PBT and the DGEBA resin first leads to the extension of the PBT chains and to the appearance of lateral hydride groups along these chains. Next, in presence of the Zn(II) catalyst, the transesterification reaction occurs leading to cross-linking and bond exchanges.

The rotational speed of the two µcompounder screws was 100 rpm. The force exercised on the barrel initially increased and then became constant after about 5 minutes, which suggests that the cross-linking reaction was over. The melt remained for 8 minutes in the µcompounder and was then transferred to a shooting pot and injected into a mold in shape of a tensile specimen (Figure S2). During injection, the flow direction corresponds to the specimen tensile axis. More details about the synthesis protocol can be found elsewhere.[22-23]

We synthesized seven different polymers denoted V_i where the subscript designates the cross-linker (DGEBA) percentage by weight (wt%). V_0 is simply the pristine PBT. The detail of the prepared reactive mixtures is indicated in table 1. Between $V_{0.5}$ and V_2 the DGEBA wt% was increased by small increment of about 0.25%. This made it possible to analyze precisely the dependence of the vitrimer mechanical properties on the degree of cross-linking. The presence of DGEBA slightly modifies the specimen color that goes from a very light brown (V_0) to a more pronounced brown (V_2) (Figure S3).

	V_0 (Pristine PBT)	$V_{0.5}$	$V_{0.75}$	V_1	$V_{1.27}$	$V_{1.56}$	V_2
Pristine PBT	100g	100g	100g	100g	100g	100g	100g
DGEBA	0g	0.5g	0.75g	1g	1.27g	1.56g	2g
Zn(II)	0g	0.1g	0.15g	0.2g	0.254g	0.31g	0.4g
Irganox	0.1g	0.1g	0.1g	0.1g	0.1g	0.1g	0.1g

Table 1 The different V_i vitrimers compositions

1.2 Mechanical testing

The measurements were performed on a Bose 3000 tensile machine equipped with a thermal chamber (Figure S4). The dog bone specimens (see Figure 1a and 1b) includes a 4×4×4 mm^3 cubic central part and were specifically designed so that necking is always initiated in the specimen center. The relative speed of the tensile machine crossheads was 0.02 mms^{-1} during the tests. The tensile machine upper limit for the grip relative displacement is 20 mm and the tests were stopped when this limit was reached. The tensile experiments were performed for the 7 V_i materials (see Table 1) at 80°C, 100°C, 130°C and 160°C. These temperatures are above the PBT glass transition temperature (T_g≈60°C) and

below the melting temperature (T_m≈225°C). In these conditions, these materials show no brittle behavior and can be deformed to very large strains.

As it is customary in continuum mechanics, a material point is identified by its initial position X (undeformed or Lagrangian coordinate) on the undeformed specimen. The current position of the X material point at time t is denoted $x(X,t)$ (deformed or Eulerian coordinate). The origin was chosen so that $x = X = 0$ corresponds to the specimen center where necking is initiated. The material points that are initially situated in the central cube of the undeformed specimen are identified during the tensile test as belonging to the $X \in [-2 \quad +2] mm$ interval. Obviously, during tensile testing, if $|X| > 0$ and $t > 0$, then $|x(X,t)| > |X|$. In order to perform 3D DIC displacement and strain measurements, a random speckle pattern was applied on the specimen surface by projecting small black paint droplets with an airbrush. The images were recorded by each of the two cameras every 1s through a glass window placed on the oven front face (Figure S4). ε is the local true strain defined by $\varepsilon(x,t) = \ln\left(\frac{dx}{dX}\right)$. dX is the initial size of a very small length element taken along the longitudinal axis and dx is its current size during the test. The maximum strain in the neck center is denoted ε^M. The nominal and true stresses are defined by $\sigma_N = F/S_0$ and $\sigma = F/S$ respectively. F is the tensile force. S_0 and S are the initial and current areas of the central cross-section. Assuming an isochoric deformation process, it can readily be checked that the true stress in the neck center is given by $\sigma = \sigma_N \exp(\varepsilon^M)$.

A strain map example is shown in Figure 1c. It corresponds to a measurement obtained during a test performed on the pristine PBT (V_0) at 80°C. In Figure 1d, we have also represented the strain profile $\varepsilon(x)$ that was directly measured along the deformed specimen. With the displacement measurement, $u(X,t) = x - X$, it is easy to obtain the strain $\varepsilon(X,t)$ as a function of the undeformed coordinate (X)—i.e., in the Lagrangian description. In Figure 1d, we have added the $\varepsilon(X)$ profile, which is logically narrower than $\varepsilon(x)$. ΔX is the full width at half maximum of $\varepsilon(X)$ (see Figure 1d). By definition ΔX is relative to the undeformed state and can therefore be considered as a measure of the material mass that is included in the most deformed part of the neck; the smaller ΔX, the more localized the strain.

The strain rate associated with a given material point—identified by X—was calculated by centered differences: $\dot{\varepsilon}(X,t) = \frac{\varepsilon(X,t+\Delta t) - \varepsilon(X,t-\Delta t)}{2\Delta t}$

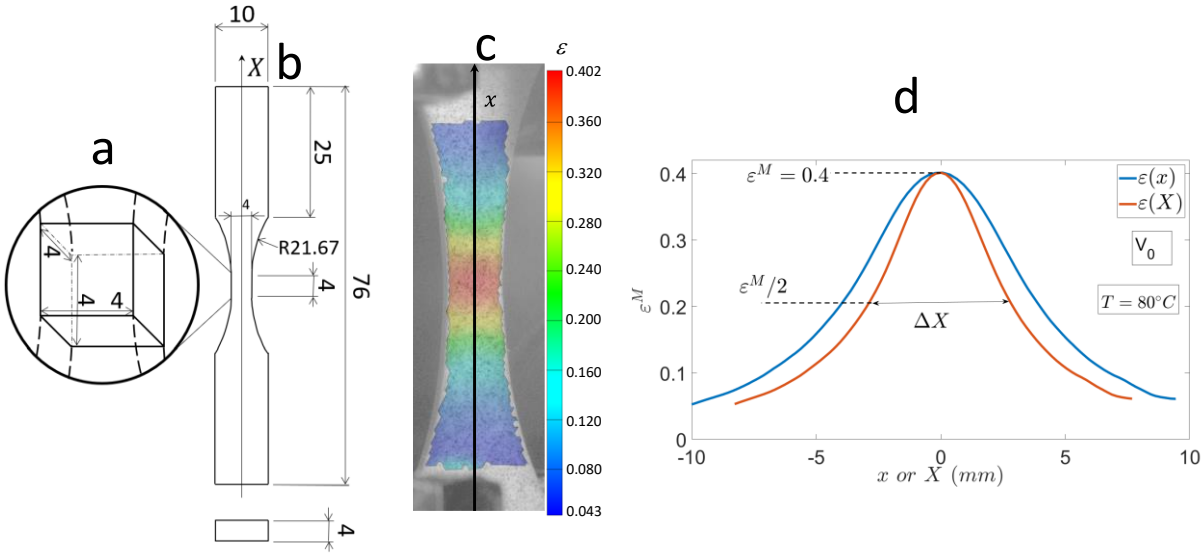

Figure 1 Strain measurement at the surface of a tensile specimen: central specimen cubic part (a), drawing of the specimens (b), strain map measured when $\varepsilon^M = 0.4$ *(c) and strain profiles along the specimen length against the Eulerian (* x *) and Lagrangian (* X *) coordinates (d).*

1.3 Dynamic Mechanical Analysis (DMA) experiments

DMA experiments were performed in tension mode using a Metravib+300 analyzer at a heating rate of 1°C/min from the room temperature to 250°C. The specimen dimensions were 20×10×4 mm^3. The amplitude and frequency of the applied tensile strain were 0.25×10^{-3} and 10Hz respectively.

1.4 Small Angle X-ray Scattering (SAXS) experiments

The SAXS measurements were performed on the SWING beamline at the Soleil synchrotron. The wavelength (λ) was 0.077489 nm and the q range ($q = \frac{4\pi \sin\theta}{\lambda}$, θ : Bragg's angle) corresponding to the patterns presented in this study is [0.12—1.8]nm^{-1}.

2 Results and Discussion

2.1 DMA Characterization of vitrimers

In Figure 2, we show the dependence of the storage modulus (E') measured by DMA versus temperature for V_0 (pristine PBT), V_1 and V_2. As for V_0, the curve evolution is in line with what is expected for a semi-crystalline polymer. The glass transition occurs at about 50-60°C. Next, E' slightly decreases. Due to the presence of the crystalline network, the material is still in the solid state. Melting begins at about 220°C and E' abruptly drops below our apparatus measurement range. At temperatures smaller than 200°C, the V_1 and V_2 vitrimer behaviors are roughly the same as that of the pristine PBT. The melting temperatures (T_m) of the two vitrimers are slightly smaller compared to V_0. Above T_m, the vitrimer behaviors drastically differ from that of the pristine PBT: a rubber plateau appears on the vitrimer E' curves (see the inset in the central part of Figure 2). The level of this plateau is rised when the vitrimer DGEBA wt% is increased. This proves that the addition of the DGEBA resin in the µcompounder has actually led to the vitrimer cross-linking, and that the degree of cross-linking depends directly of the DGEBA wt% as it has already been demonstrated in previous works.[22]

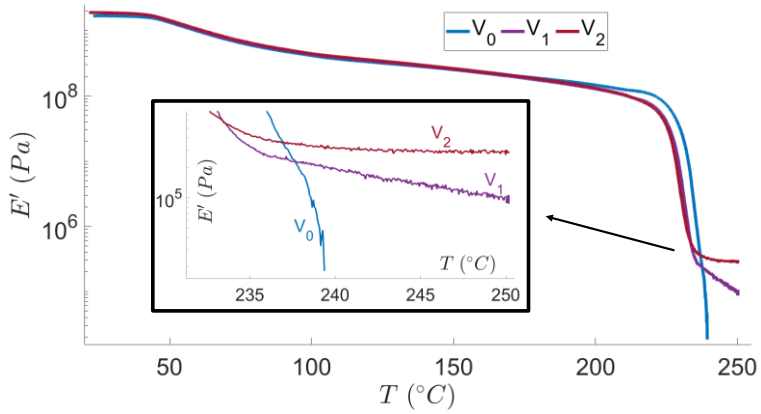

Figure 2 E' (storage modulus) versus temperature for V_0, V_1 and V_2.

2.2 Characteristic tensile curves and definition of the strain range of plastic instability

The main objective of this part is to highlight and analyse through full-field strain (ε) and strain rate ($\dot{\varepsilon}$) measurements the successive strain localization and delocalization stages that can occur during the plastic deformation process. Based on these observations, we were able to objectively identify the high and low bounds of the strain range of plastic instability—strain range during which strain localization occurs and neck develops.

The σ_N versus ε^M curve measured for V_0 at 80°C is shown in Figure 3. This curve exhibits a maximum at the yield strain $\varepsilon^M = \varepsilon_Y = 0.19$, and a minimum at $\varepsilon^M = \varepsilon_{NS} = 0.71$. In Figure 4, we have plotted the $\dot{\varepsilon}$ curves measured at the beginning of the test for different material points situated in the specimen central part (X=0, 0.4 mm, 0.6 mm, 0.8 mm and 1.0 mm). Initially, the strain rates are the same for all these material points. The curves begin to separate when strain localizes, then $\dot{\varepsilon}$ becomes maximum in the specimen center (X=0), which is observed approximately at the yield point ($\varepsilon_Y = 0.19$). This confirms that the lower bond of the strain range of plastic instability is the yield strain ε_Y (first Considère condition, defined at σ_N maximum).

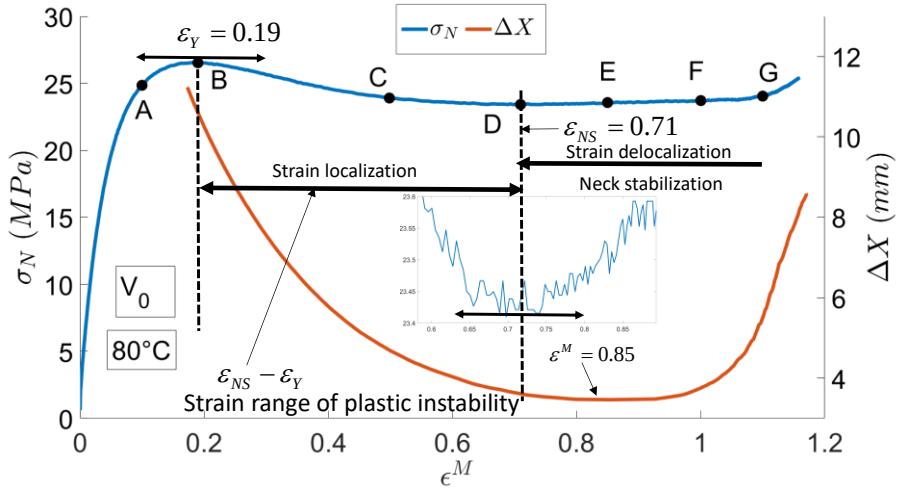

Figure 3 σ_N and ΔX versus ε^M for V_0 at 80°C. Inset: zoom around point D on the $\sigma_N(\varepsilon^M)$ curve.

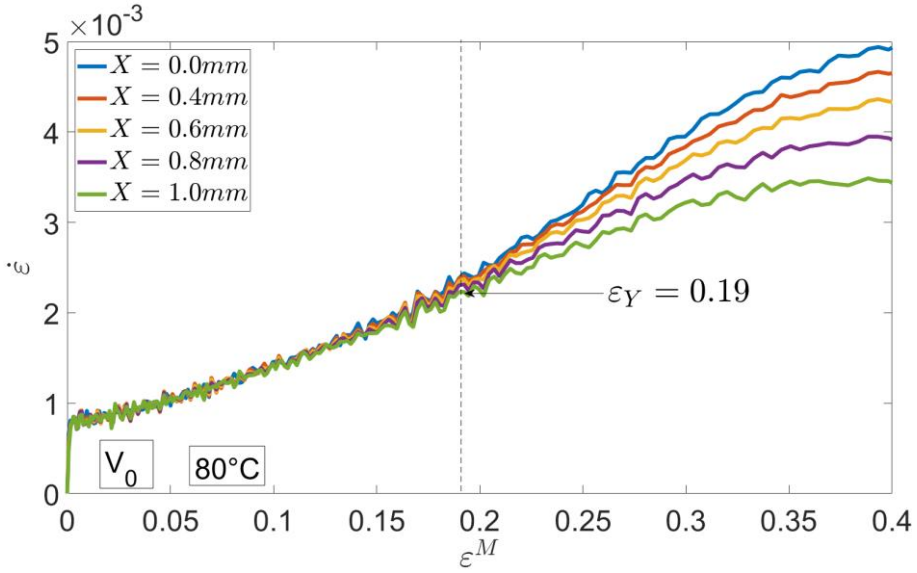

Figure 4 Strain rate curves $\dot{\varepsilon}$ obtained at the beginning of the tensile test for different material points situated in the specimen central flat part (V_0, 80°C).

In Figure 5, we show the strain rate ($\dot{\varepsilon}$) profiles that were measured along the specimen length, which we plot here as function of the Lagrangian coordinate X. The first profile was obtained before the yield point, at point A ($\varepsilon^M = 0.1$) of the $\sigma_N\left(\varepsilon^M\right)$ curve (Figure 3). This strain rate profile is nearly constant in the specimen central part, which confirms that strain localization has not taken place. The slight decrease observed at either side of the curve is due to the variation of the cross-section along our dog bone specimen. For the yield point B ($\varepsilon^M = \varepsilon_y = 0.19$), strain localization has started and the $\dot{\varepsilon}$ profile clearly becomes sharper. For point C, ($\varepsilon^M = 0.5$), the narrowing of the peak width has become more pronounced and the strain rate in the center has more than doubled. This trend has been reversed at the nominal stress minimum (point D, $\varepsilon^M = \varepsilon_{NS} = 0.71$)): the strain rate curve has broadened and the strain maximum in the specimen center has significantly decreased. At strains slightly larger than $\varepsilon_{NS} = 0.71$, neck stabilization can be observed simply and directly thanks to our 3D DIC measurements: The strain rate maximum is no longer situated in the neck center but in two symmetrical points around the center. This is barely observable for the strain rate profile measured at $\varepsilon^M = 0.85$, but it is clear at $\varepsilon^M = \varepsilon^1_{NS} = 0.87$ (see the inset in the right upper part of Figure 5). In the following, we note ε^1_{NS}, the minimum value of ε^M for which we detected that the strain rate maximum is no longer in the specimen center, but in two symmetrical points on each side of the center.

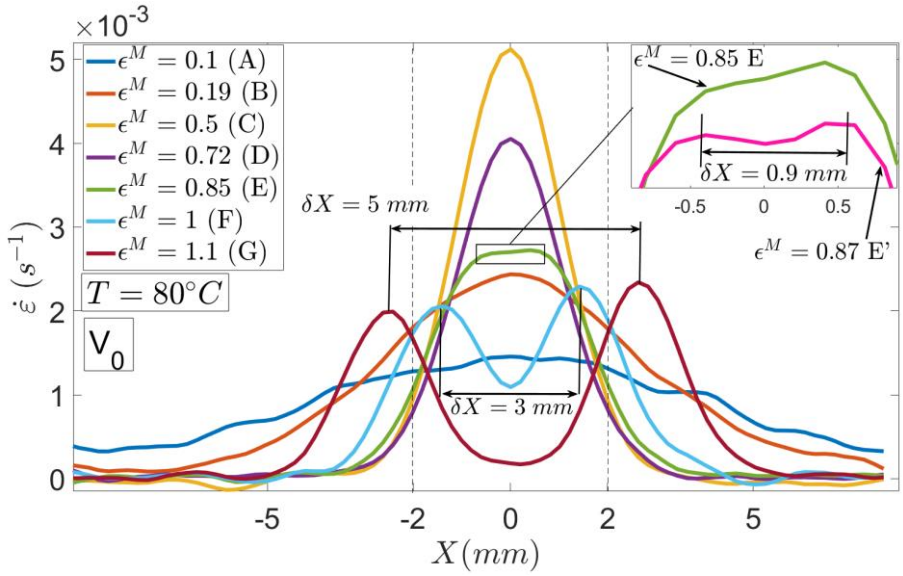

Figure 5 Strain rate profiles $\dot{\varepsilon}$ against the Lagrangian coordinate X for different selected ε^M strains corresponding to the states indexed by points A to G in Figure 3 (V_0 at 80°C).

The Lagrangian quantity δX is the distance on the undeformed specimen between the two material points where the stain rate is maximum. Note that δX defined in Figure 5 is different from ΔX defined in Figure 1d. During neck stabilization, δX increases: $\delta X = 0.9mm$ at $\varepsilon^M = 0.87$, $\delta X = 3mm$ at $\varepsilon^M = 1$ and $\delta X = 5mm$ at $\varepsilon^M = 1.1$ (see Figure 5). It can be checked that the two symmetrical maxima that appear on the strain rate profiles when $\varepsilon^M > \varepsilon_{NS}^1$ correspond to material points that are situated in the neck shoulders at the time of measurement.[6,7] Therefore, the δX increase means that the neck gradually extends to all the material points of the specimen. At the end of the test, $\delta X > 4mm$: the strain rate maxima—and therefore the neck shoulders—correspond then to material points situated outside the central cube that can be seen on the undeformed specimen. (see Figure 1a).

By analyzing the evolution of the ΔX variable during the test (see the definition of ΔX in Figure 1d), it is possible to confirm that neck stabilization has begun at ε_{NS}^1. Initially, ΔX decreases, which is the combined effect of stress inhomogeneity due to specimen geometry, initial material softening, and strain localization after the yield point. For $\varepsilon^M = 0.85 \approx \varepsilon_{NS}^1$, ΔX reaches a minimum and then rises. Logically, when the strain rate is no longer maximum at the material point located in the specimen center, the bell curve of strain in the Lagrangian description ($\varepsilon(X)$, Figure 1d) begins to broaden. The quantity of substance (i.e., the mass) included in the specimen most deformed part increases: the neck extends toward the less deformed regions of the specimen; neck stabilization is in progress.

With our 3D DIC measurements—i.e., through direct observation of strain delocalization—we have defined a threshold strain, ε_{NS}^1, characterizing the neck stabilization beginning. ε_{NS}^1 was found to be slightly larger than ε_{NS}, which was also checked for all the tests performed during this study (see section 2.4.3). We have therefore decided to set the upper bound of the strain range of plastic instability to ε_{NS}—i.e, at the nominal stress minimum, which is in accordance with the second Considère condition. In the following, we will consider that the strain range of plastic instability extends from ε_Y to ε_{NS}. However, the conclusions of the study would have been the same if we had chosen ε_{NS}^1 for the upper bound of this interval. Let us note that ε_{NS} corresponds to the definition of the natural draw ratio as given by Ward and Sweeney[1] or Séguéla[2].This quantity is closely related to strain hardening and its measurement makes it possible to compare the limitation in extensibility of polymers. These points will be illustrated in section 2.4.3.

The definition of the strain range of plastic instability was introduced by analyzing the tensile behavior of the pristine PBT (V_0), which exhibits significant strain localization. We will now examine the opposite case of the V_2 vitrimer. The evolution of the nominal stress measured at 160°C for V_2 shows nor maximum neither minimum (Figure 6), which suggests that deformation occurs in a quasi-uniform way

along the specimen. This is confirmed by the analysis of the strain rate profiles (inset in Figure 6) that are nearly constant throughout the test in the specimen central flat part. Compared to Figure 5, the curves in the Figure 6 inset appear to be noisy. This is due to the reduced contrast between the black paint and the V_2 specimen brown surfaces (see Figure S3), moreover accentuated by the fact that the maximum of the strain rate scale is five times smaller in the inset of Figure 6 than in Figure 5.

We have briefly presented the two extreme deformation processes possible for our materials: The first behavior type is called "YPTC" (Yield Point on the Tensile Curve, see V_0 at 80°C) in the following and is associated with pronounced successive stages of strain localization and delocalization. The second behavior type is hereinafter referred as to "NYPTC" (No Yield Point on the Tensile Curve, see V_2at 160°C) and corresponds to quasi-uniform deformation during the test. In the following, we performed several tests at various test temperatures and for vitrimers synthesized with various DGEBA wt% in order to study carefully the transition between these two characteristic behaviors.

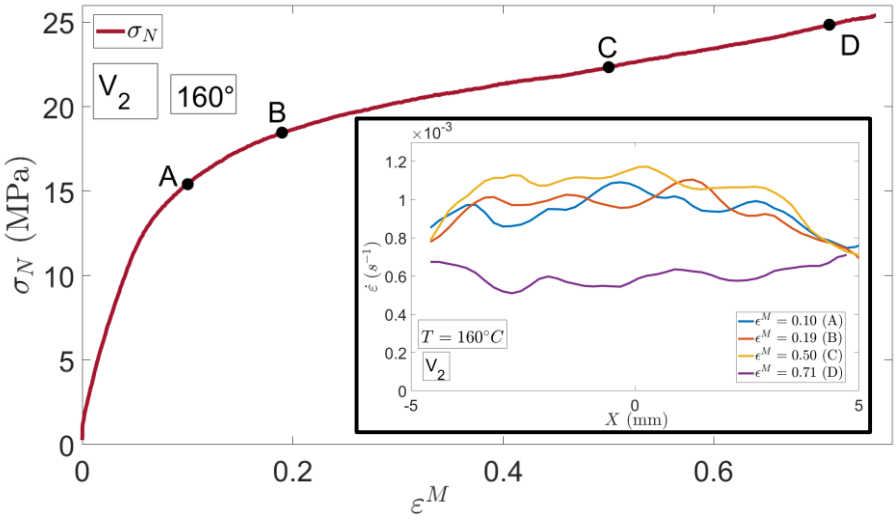

Figure 6 σ_N versus ε^M for V_2 at 160°C. The strain rate profiles $\dot{\varepsilon}(X)$ measured at points A, B, C and D are shown in the inset.

2.3 Influence of cross-linking on the vitrimer mechanical behavior

In Figure 7, we show the evolution of the nominal stress σ_N against ε^M for all the V_i materials and test temperatures (80°C: Figure 7a, 100°C: Figure 7b, 130°C: Figure 7c and 160°C: Figure 7d). Similarly, the true stress-true strain curves ($\sigma(\varepsilon^M)$) are plotted in Figure 8. The effect of cross-linking is easy to observe on the curves shown in Figure 7 and 8: At the four test temperatures, the higher the DGEBA content—and thus the degree of cross-linking—the larger the stress. It should be noted that the strain rates $\dot{\varepsilon}^M$ are not the same for the different materials during the tests. The strain rate becomes smaller

when the degree of cross-linking increases (see Figure S5 for the tests performed at 80°C). It is well known that the stress increases when the strain rate is increased. If the tests would had been carried out at a same constant strain rate—for example: 2.5 10^{-3} s^{-1}, roughly the average values of the curves of Figure S5—the curves shown in Figure 8 would have been slightly modified. Nevertheless, the effect of cross-linking would have been even more noticeable since the gaps between the curves would have increased. We have also calculated the evolution of the strain hardening coefficient[4,24] $\gamma\left(\varepsilon^M\right)=\frac{\ln\sigma}{d\varepsilon^M}$ as a function of ε^M. This coefficient is independent of strain rate if the true strain-true stress relationship can be written in the general form: $\sigma\left(\varepsilon,\dot{\varepsilon}\right)=f\left(\varepsilon\right)g\left(\dot{\varepsilon}\right)$ as it is the case for the phenomenological G'sell and Jonas model that is widely used for describing the tensile behavior of semi-crystalline polymers.[24-25] The $\gamma\left(\varepsilon^M\right)$ curves presented in Figure S6 confirm that an increase in DGEBA wt% leads to an increase in strain hardening, an expected consequence of cross-linking.[26-27]

The Figures 7 and 8 curves show that the tensile properties of vitrimers can be precisely tuned by controlling the cross-linker concentration. The V_{05} and V_0 nominal stress curves are very close but the effect of cross-linking can still be demonstrated through the γ strain hardening coefficient that is higher for V_{05} than for V_0 (see Figure S6). Furthermore, at the end of the tensile test, an abrupt increase of the stress can be observed for V_0 and V_{05} at the four temperatures (see the arrows at the end of the Figure 7 curves). This may correspond to the high strain range when the polymer chain are in full-extension.[28] The final stress increase always occurs at smaller strains for V_{05} than for V_0. This suggests that the molecular network was indeed modified, and that the node density is larger for V_{05} than for V_0. Recrystallization that was already observed for PBT at large strains could also contribute to the final stress increase visible in the Figure 8 curves.[29]

The transition between the YPTC behavior and the NYPTC behavior with the increases in DGEBA wt% can be seen at the four temperatures on the curve sets shown in Figure 7. At 80°C for example, the V_0, $V_{0.5}$ and $V_{0.75}$ curves clearly exhibit a yield point. By enlarging the corresponding curves, it can be checked that this remains true for V_1 but not for $V_{1.27}$. At 100°C, the transition is also observed between the V_1 and $V_{1.27}$ curves. The transition is between the $V_{0.75}$ and V_1 curves at 130°C and 160°C. The evolution between the YPTC and NYPTC behaviors takes place in a very gradual or continuous manner. This is well illustrated for the measurements performed at 160° where the $V_{0.75}$ (YPTC behaviour) and V_1 (NYPTC behavior) curves are very close and look the same if they are not enlarged.

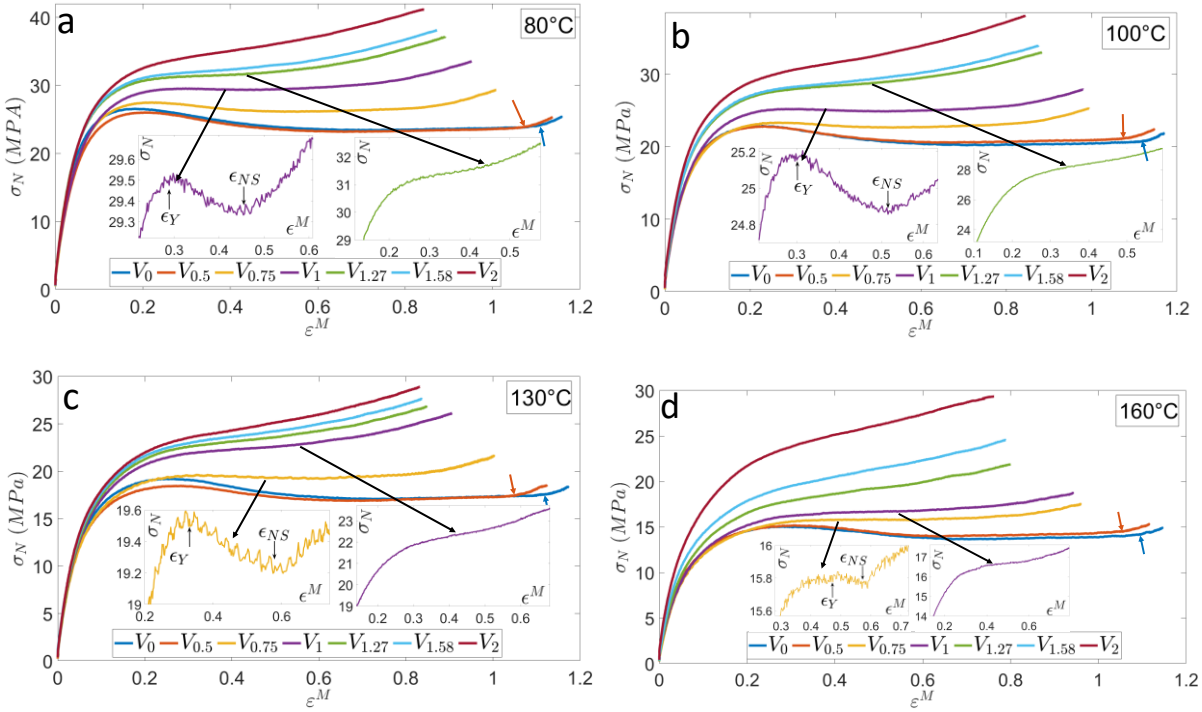

Figure 7 $\sigma_N\left(\varepsilon^M\right)$ curves, a: 80°C, b: 100°C, c : 130°C and d: 160°C.

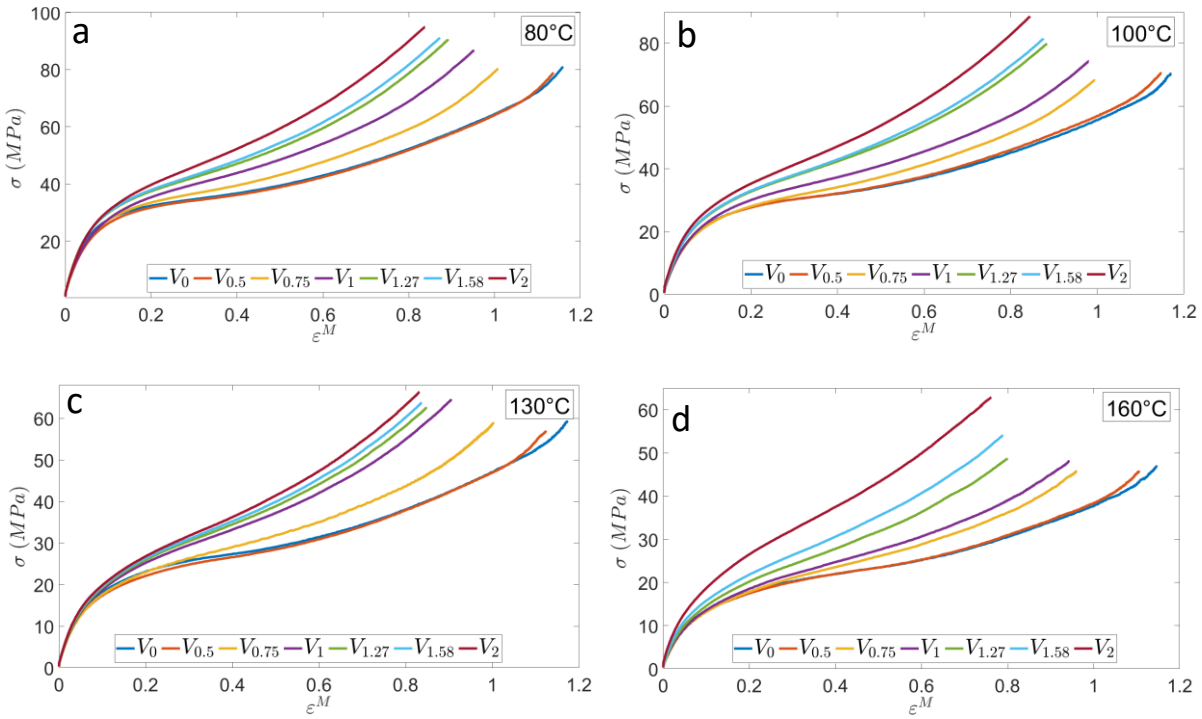

Figure 8 $\sigma\left(\varepsilon^M\right)$ curves, a: 80°C, b: 100°C, c : 130°C and d: 160°C.

2.4 Dependence of strain range of plastic instability on cross-linking

2.4.1 Increase of the lower bound (ε_Y)

The yield strain (ε_Y) and stress (σ_Y) values are reported in table 2 (line 2 and 3) for all the test temperatures. As expected, when the test temperature of a given V_i material increases, the yield strain increases and the yield stress decreases. More interestingly, it can be checked that the higher the DEGBA concentration, the higher the yield strain—i.e., the higher the strain localization onset (see line 3 of Tables 2a, 2b, 2c and 2d). Instead, we would have expected the cross-linking to hinder the polymer deformation and thus result in lower yield strains (ε_Y). A literature review was conducted to clarify this apparent contradiction. We found that the yield strain (and stress) of a semi-crystalline polymers may strongly depend on the initial orientation degree of the material.[30-31] To assess whether our materials exhibited some degree of pre-orientation, we carried out SAXS experiments on our samples.

2.4.2 Effect of Pre-orientation

The SAXS patterns measured for the undeformed V_0, V_{05}, V_1, $V_{1.5}$ (DGEBA wt%1.5%≈1.58%) and V_2 polymers are shown in Figure 9. The X-ray beam passed through the specimens along the thickness direction. The diffuse ring associated with the spherulitic morphology is clearly visible on the V_0 and V_{05} patterns. In Figure 10, we show the intensity profiles measured along the rings corresponding to $q = q^h_{\max} = cte$, where $q^h_{\max}$ is the value at maximum intensity along the horizontal axis. For V_0, $V_{0.5}$, V_1, $V_{1.5}$, and V_2, the $q^h_{\max}$ values are 0.52, 0.50, 0.44 ,0.43 and 0.42 nm^{-1} respectively. The profiles of Figure 10 reveals that V_0 and V_{05} are weakly anisotropic, and that the anisotropy is slightly more pronounced for V_{05} than for V_0. On the other hand, the V_1, $V_{1.5}$ and V_2 patterns are strongly anisotropic (note the log scale for the y axis in Figure 10), and are characteristic of the presence of a "shish-kebab" type morphology.[32-33] The "shish-kebab" morphology is induced by shear at the mold walls during polymer injection and is concentrated in the specimen skin regions. The increase in shear stress at the mold walls is due to the increase in polymer viscosity caused by cross-linking. In the case of polymers with high viscosities, the occurring of oriented morphologies is inherent to the injection process and must be taken in consideration when implementing this type of shaping process. Moreover, it was shown in previous studies that the shish kebab morphology is preserved when the polymer is annealed below, near or above the melting temperature.[34] Accordingly, after annealing the polymer remains strongly oriented.

In short, when the degree of cross-linking is increased, the material degree of pre-orientation increases as well (see Figure 10), which contribute to increase the yield strain as already reported in published works.[30,31] The material pre-orientation degree seems to have a significant influence on the tensile properties. This can be illustrated by analyzing the behaviors of the V_0, $V_{0.5}$ and V_1 materials. The V_0

and $V_{0.5}$ SAXS patterns are very similar (see Figure 9 and 10) and the tensile properties of these two materials are also nearly the same (see Figure 7 and 8). On the other hand, the V_1 SAXS pattern differs significantly from those of V_0 and $V_{0.5}$, so is its tensile behavior.

80°C	V_0	$V_{0.5}$	$V_{0.75}$	V_1	$V_{1.27}$	$V_{1.56}$	V_2
σ_Y (MPa)	26.51	25.98	27.46	29.51	NM	NM	NM
ε_Y	0.19	0.21	0.22	0.30	NM	NM	NM
σ_{NS} (MPa)	23.42	23.19	26.14	29.33	NM	NM	NM
ε_{NS}	0.71	0.67	0.54	0.45	NM	NM	NM
ε_{NS}^1	0.87	0.84	0.65	0.58	NM	NM	NM

Table 2a

100°C	V_0	$V_{0.5}$	$V_{0.75}$	V_1	$V_{1.27}$	$V_{1.56}$	V_2
σ_Y (MPa)	22.82	22.04	23.29	25.19	NM	NM	NM
ε_Y	0.23	0.24	0.27	0.30	NM	NM	NM
σ_{NS} (MPa)	20.22	20.60	22.63	24.86	NM	NM	NM
ε_{NS}	0.73	0.63	0.54	0.52	NM	NM	NM
ε_{NS}^1	0.89	0.77	0.66	0.61	NM	NM	NM

Table 2b

130°C	V_0	$V_{0.5}$	$V_{0.75}$	V_1	$V_{1.27}$	$V_{1.56}$	V_2
σ_Y (MPa)	19.17	18.42	19.6	NM	NM	NM	NM
ε_Y	0.26	0.28	0.33	NM	NM	NM	NM
σ_{NS} (MPa)	17.21	17.06	19.31	NM	NM	NM	NM
ε_{NS}	0.76	0.68	0.60	NM	NM	NM	NM
ε_{NS}^1	0.9	0.82	0.66	0.58	NM	NM	NM

Table 2c

160°C	V_0	$V_{0.5}$	$V_{0.75}$	V_1	$V_{1.27}$	$V_{1.56}$	V_2
σ_Y (MPa)	15.03	14.90	15.80	NM	NM	NM	NM
ε_Y	0.28	0.33	0.48	NM	NM	NM	NM
σ_{NS} (MPa)	13.65	13.78	15.73	NM	NM	NM	NM
ε_{NS}	0.70	0.69	0.58	NM	NM	NM	NM
ε_{NS}^1	0.84	0.84	0.69	0.62	NM	NM	NM

Table 2d

Table 2 Mechanical properties of PBT (V_0) and PBT-based vitrimers (V_i, $i \neq 0$), a: 80°C, b: 100°C, d: 130°C and d: 160°C. NM: Not Measurable.

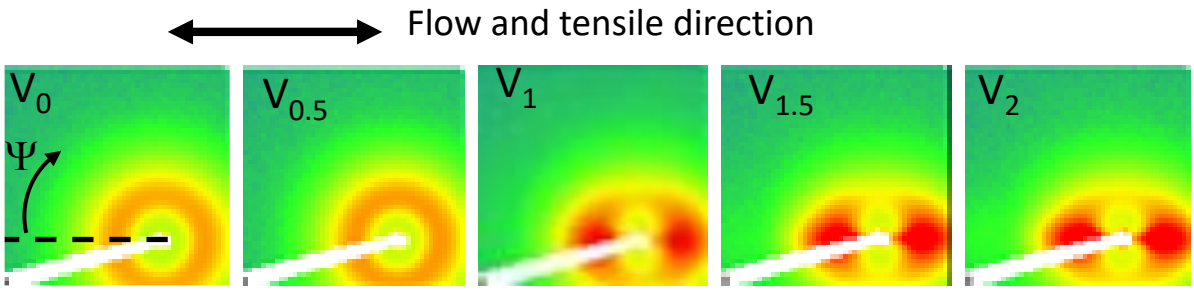

Figure 9 SAXS Patterns measured before deformation for V_0, $V_{0.5}$, V_1, $V_{1.5}$ (DGEBA wt%=1.5≈1.58) and V_2.

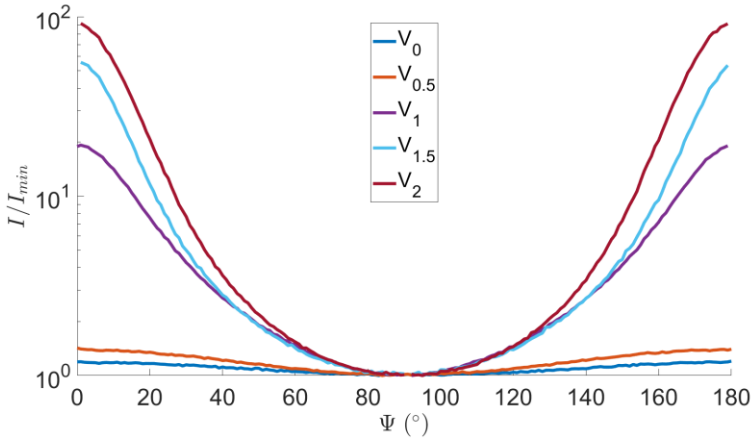

Figure 10 Intensity profiles versus Ψ (azimuthal angle, defined on the V_0 pattern in Figure 9) at $q = q^h_{\max}$ ($q^h_{\max}$ maximum intensity along the horizontal axis). The intensity is normalized by the minimum value ($I_{\min}$) along the profile and averaged on a ±0.05 nm^{-1} interval around $q^h_{\max}$.

2.4.3 Decrease of the upper bound (ε_{NS})

ε_{NS} and ε^1_{NS} that correspond to characteristic steps of the neck stabilization phase beginning (see section 2.2) are reported in lines 5 and 6 of table 2. For V_1 at 130°C and 160°C, the measurement of ε^1_{NS} may remain possible even if the nominal stress curve exhibit no maximum or minimum values, which suggests that moderate localization/delocalization effects may still be present. This is to be confirmed by the analysis of the ΔX curves (see section 2.4.5). ε_{NS}, ε^1_{NS} and ε_Y are plotted in Figure 11 as a function of the DGEBA wt%. As in the case of the test analyzed in the 2.2 section (V_0 at 80°C), ε^1_{NS} is always slightly larger than ε_{NS}, and the difference is very roughly constant: $\varepsilon^1_{NS} - \varepsilon_{NS} = 0.11 \pm 0.05$. This confirms the conclusion of section 2.2: strain delocalization is objectively observed shortly after ε_{NS}. Neck stabilization occurs approximately at this strain value. It is well reasonable to consider that ε_{NS} is the upper bound of the strain range of plastic instability.

At the four test temperatures, the same trend is observed for ε_{NS} and ε_{NS}^{1} (Figure 11): the higher the DGEBA concentration—and therefore the degree of cross-linking—the smaller the ε_{NS} and ε_{NS}^{1} values, which shows that neck stabilization (strain delocalization) occurs at smaller strains for the strongly cross-linked polymers. As previously mentioned, ε_{NS} can be seen as an indicator of the polymer limitation in extensibility. This is illustrated and commented in Figure S7 where the evolution of ε^{M} is represented for V_0, $V_{0.5}$, $V_{0.75}$ and V_1 at 80°C. In this figure, it can be checked that the lower ε_{NS}, the lower the level of the plateau where "strain saturation" (limitation in extensibility) is observed. Furthermore, by analyzing the $\gamma\left(\varepsilon^{M}\right)$ (strain hardening coefficient) curves it can also be understood that an increase in strain hardening results in a decrease of ε_{NS}. Assuming an isochoric deformation process, the true stress writes $\sigma = \sigma_N \exp\left(\varepsilon^{M}\right)$ and it is easy to show that $d\sigma_N = 0 \Leftrightarrow \gamma = 1$. In the case of the YPTC behavior, $\gamma\left(\varepsilon^{M}\right)$ crosses the $\gamma = 1$ curve twice. The first time during its decreasing part at the yield point (σ_N maximum) for $\varepsilon^{M} = \varepsilon_Y$, and the second time during the increasing part that follows, at neck stabilization (σ_N minimum) for $\varepsilon^{M} = \varepsilon_{NS}$ (see V_0 at 80°, Figure S6). Therefore, when the $\gamma\left(\varepsilon^{M}\right)$ curve is shifted upward (increase in strain hardening) the ε_{NS} value becomes smaller.

Two complementary effects occurring at the macromolecular network level can explain the increase in strain hardening leading to the decrease of the strain at neck stabilization as observed when the degree of cross-linking is rised: Firstly, due to cross-linking, "chemical" nodes are added to the "physical" entanglements nodes (see Figure S1). The network node density increases, which results in a reduction of the intrinsic molecular network extensibility and therefore in a reduction of the strain level at which neck stabilization occurs. Secondly, the polymer pre-orientation can be seen as a prior extension in the melt. Before applying, the tensile stress ($\varepsilon^{M} = 0$), the macromolecular network is already stretched, which limits the strain increment that is necessary to reach the network limitation in extensibility. The influence of the pre-orientation degree on the limitation in extensibility of semi-crystalline polymers is reported in several published works.[13-15]

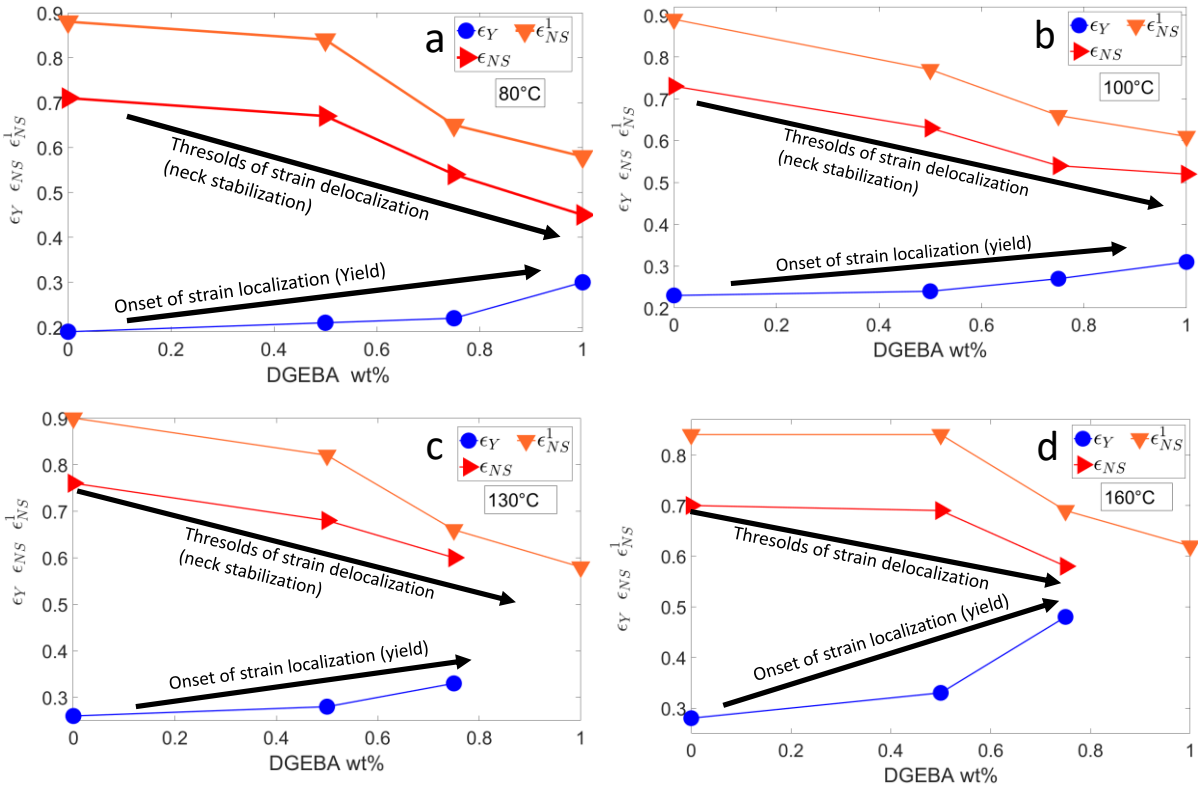

Figure 11 DGEBA wt% dependence of the yield strain (ε_Y , onset of strain localization), and of the strain delocalization thresholds (ε_{NS} , ε_{NS}^1), a: 80°C, b: 100°C, c : 130°C and d: 160°C.

2.4.4 Effects of temperature and strain rate

In the explanation concerning the decrease of the strain at neck stabilization with cross-linking that we provide at the end of the previous section (section 2.4.3), we have only considered the influence of the network topological characteristics. We also wanted to assess the possible effect of temperature or strain rate. In Figures 12a and 12b, ε_{NS} and ε_{NS}^1 are plotted against the temperature for V_0, $V_{0.5}$ and $V_{0.75}$, the three materials for which these quantities are available at the four temperatures. The ε_{NS} and ε_{NS}^1 evolutions show only slight variations with temperature, without it being possible to identify a clear trend. We also carried out tensile tests at different strain rates for V_0. ε_{NS} was found to be unchanged, $\varepsilon_{NS} = 0.71 \pm 0.01$, for crosshead speeds of 0.060 mms^{-1}, 0.020 mms^{-1} and 0.0067 mms^{-1} (See Figure S8). We can note that this result is contained in the G'sell and Jonas model.[24-25] As previously mentioned, this model involves that $\gamma\left(\varepsilon^M\right)$ is independent of strain rate, the same applies to ε_{NS}, which is defined when $\gamma = 1$ (see section 2.4.3).

In short, the temperature and strain rate are only secondary effects on ε_{NS} and thus on the polymer limitation in extensibility compared to the large primary effects linked to the molecular network characteristics, namely the network node density and its pre-orientation.

It is worth noting that in the temperature range of investigation, we have not detected any rise of ε_{NS} or ε_{NS}^{1} that could indicate that a possible thermal activation of covalent bond migrations could have changed the network extensibility properties.

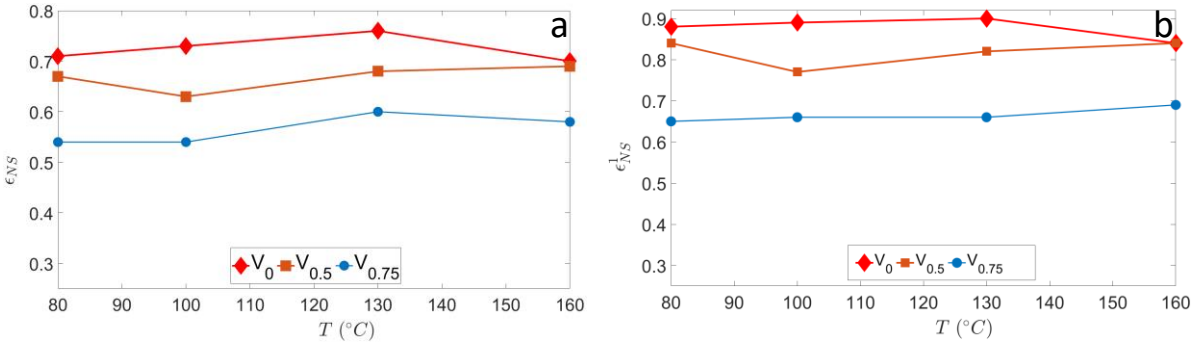

Figure 12 Temperature dependence of ε_{NS} (a) and ε_{NS}^{1} (b).

2.4.5 Gradual suppression of strain localization

The $\Delta X\left(\varepsilon^{M}\right)$ curves measured at the four test temperatures for the pristine PBT (V_0) and the V_i vitrimers are shown in Figure 13 (a: 80°C, b: 130°C) and Figure S9 (a: 100°C and b: 160°C). As illustrated in the inset of Figure 13b for strain profiles measured at 130°C when $\varepsilon^{M}=0.6$, a low ΔX value implies strong strain localization. Therefore, the curves of Figure 13 allow quick and simple comparison of the different materials cross-linking degree effect on strain localization.

Clearly, for all the curves corresponding to DGEBA concentrations lower than 1.56%: the smaller the DGEBA, the smaller ΔX. This confirms that strain localization is more pronounced when the polymer is weakly cross-linked. At 80°C (Figure 13a) the ΔX curve measured for $V_{1.27}$ is clearly below that corresponding to $V_{1.56}$ though no maximum can be observed on the corresponding nominal stress curves. This shows that moderate strain localization (necking) solely due to plastic instability—i.e., independent of specimen geometry—can occur even if no yield point appears on the nominal stress curve. This is also true at the other temperatures, for example at 130°C: the V_1 and $V_{1.27}$ tensile curves show no yield point (Figure 7c) but the V_1 ΔX curve is significantly below that of $V_{1.27}$ (Figure 13b). As for $V_{1.56}$ and V_2, the ΔX curves are very close. It can be assessed that the weak variations of these two curves are then fully dependent of the specimen geometry and the associated stress concentrations phenomena, as for any "plastically homogeneous" materials (materials that show no plastic

instability). In other words, the plastic instability leading to strain localization is completely suppressed for the vitrimers with the highest cross-linking degrees. All the ΔX curves increase at the end tests. As previously mentioned, this indicates the occurring of strain delocalization (see section 2.2). We placed symbols (filled circles) to indicate the ΔX curve minima in Figure 13. It can be checked that the strain at these minima are logically close to the ε_{NS}^{1} values reported in Table 2 (line 6). The strains corresponding to these minima decrease when the DGEBA wt% increases. This confirms again that neck stabilization occurs at lower strains when the polymer degrees of cross-linking are increased.

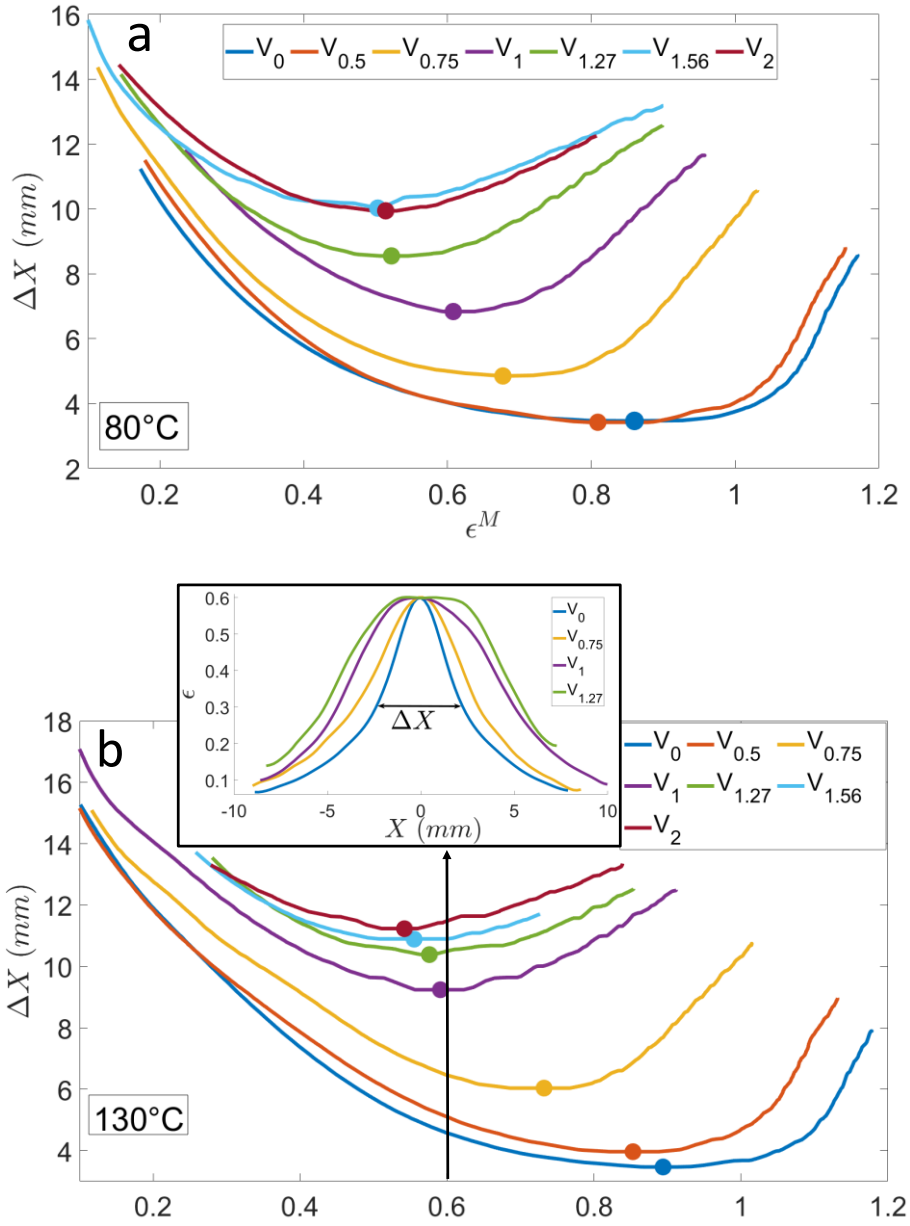

Figure 13 Evolutions of ΔX against ε^{M} at 80°C (a) and 130°C (b).

2.4.6 Summary of our results

For the investigated polymers, the strain localization/delocalization phenomena can be summarized as follows. When the DGEBA concentration is increased: 1) the yield strain increases slightly (ε_Y , strain localization onset), and 2) neck stabilization occurs at much smaller strains (ε_{NS} and ε_{NS}^1 , strain delocalization beginning). When the material is highly cross-linked, the strain at neck stabilization becomes very close to the yield strain and the strain range of plastic instability ($\varepsilon_{NS}-\varepsilon_Y$) decreases (see Figure 14). Eventually, when it vanishes ($\varepsilon_{NS}-\varepsilon_Y \to 0$), this leads to the suppression of the nominal stress mimimum and maximum on the $\sigma_N\left(\varepsilon^M\right)$ curves. This is illustrated at 80°C in the inset of Figure 14. It can also be checked in table 2 that the yield stress (σ_Y , line 2) and the nominal stress (σ_{NS} , line 4) at neck stabilization become very close on the last curve for which the YPTC behavior is observable: $\sigma_Y-\sigma_{NS}\approx 0.18\,MPa$ for V_1 at 80°C, $\sigma_Y-\sigma_{NS}\approx 0.33\,MPa$ for V_1 at 100°C, $\sigma_Y-\sigma_{NS}\approx 0.29\,MPa$ for $V_{0.75}$ at 130°C. As for $V_{0.75}$ at 130°C, $\varepsilon_{NS}^1-\varepsilon_{NS}$ is very small, about (≈ 0.1); then $\sigma_Y-\sigma_{NS}\approx 0.07\,MPa$ and the YPTC behavior is hardly noticeable.

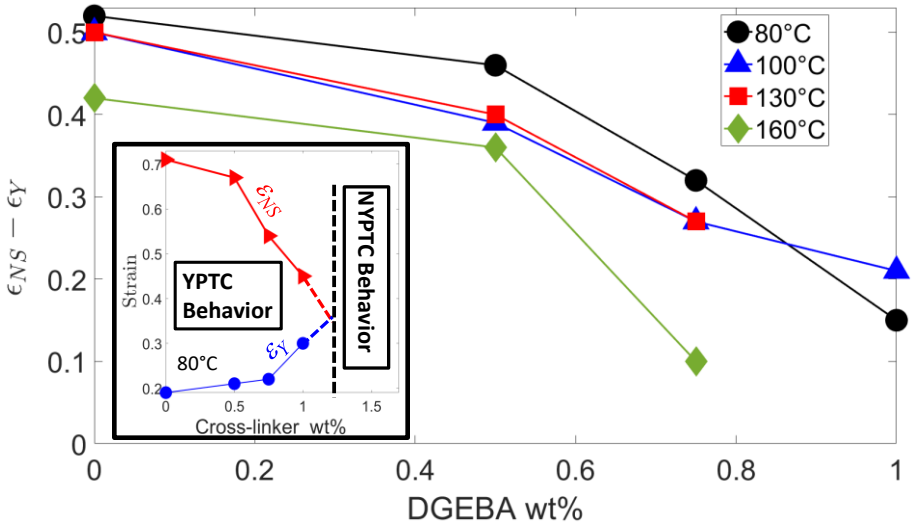

Figure 14 Strain range of plastic instability ($\varepsilon_{NS}-\varepsilon_Y$) versus the DGEBA wt%. The inset illustrates the mechanism leading to the transition between the YPTC and NYPTC behaviors.

Conclusion

The chief goal of this study was to investigate finely the influence of cross-linking on the mechanical properties of PBT-based vitrimers produced by injection molding. We carried out tensile tests at

various temperatures coupled with full-field strain measurements on vitrimers whose cross-linker concentrations have been changed in very small increments. We found that the strain range of plastic instability—phase during which strain localization occurs—decreases when the degree of cross-linking is increased. This gradually leads to the suppression of necking. The reduction of the strain range of plastic instability is mainly due to the decrease of the strain threshold (ε_{NS}) at which neck stabilization begins.

At the microstructure level, the decrease of ε_{NS} is due to the limitation in extensibility of the macromolecular network caused by cross-linking. When the degree of cross-linking is increased, two complementary effects contribute to the network limitation in extensibility: firstly the decrease of chain length between the nodes of the macromolecular network, and secondly the pre-orientation of this network. Pre-orientation of polymers with high cross-linking degrees and therefore with high viscosities like PBT-based vitrimers cannot be avoided in the very common case when injection molding is used to produce them. An interesting extension of this study would be to obtain our tensile specimens through a process like compression molding that preserves material isotropy. It would then be possible to study the specific tensile behavior of non-oriented vitrimers.

We also found that ε_{NS} does not depend on temperature or strain rate, which confirms that the properties of the macromolecular network is the primary factor to take into account to describe the neck stabilization characteristics.

References

1 M. Ward, J. Sweeney, *Mechanical properties of solid polymers* **2013**, Wiley third edition chap 12.

2 P. I. Vincent, *Polymer* **1960**, 1, 7.

3 A. Galeski, *Prog. Polym. Sci.* ***2003****, 28, 1643.*

4 R. Séguéla, *Macromol. Mater. Eng.* **2007**, *292*, 235.

5 B. Crist, C. Metaxas, *J. Polym. Sci. B: Polym. Phys.* **2004**, *42*, 2081.

6 J. Ye, S. André, L. Farge, *Int. J Solids Struct.* **2015**, 59, 58.

7 L. Farge, S. André, J. Boisse, *Polymer* **2018**, 153, 295.

8 F. Rietsch, R. A. Duckett, I. M. Ward, *Polymer* ***1979***, 20, 1133.

9 D. M. Bigg, Polym. *Eng. Sci.* **1988**, 28, 830.

10 S. Humbert, O. Lame, G. Vigier, *Polymer* **2009**, *50*, 3755.

11 Y. Men, J. Rieger, G. Strobl, *Phys. Rev. Lett.* **2003**, 91, 095502.

12 B. A. Schrauwen, R. P. Janssen, L. E Govaert, H. E. Meijer, *Macromolecules* **2004**, *37*, 6069.

13 J.S. Foot, I.M. Ward, *J. Mater. Sci*. **1975**, 10, 955.

14 J.P. Cavrot, F. Rietsch, *Eur. Polym. J.* **1985**, 21, 787

15 A.N. Gent, J. Jeong, Polym. Eng. Sci. **1986**, 26,285.

16 R. Séguéla, F. Rietsch, *J. Mater. Sci. Lett.* ***1990***, *9*, 46.

17 N. W. Brooks, R. A. Duckett, I. M.Ward, *Polymer* **1992**, 33, 1872.

18 D. Montarnal, M. Capelot, F. Tournilhac, L. Leibler, *Science* **2011**., 334, 965.

19 W. Denissen, J.M. Winne, F.E. Du Prez, *Chem. Sci.* **2016**, 7, 30.

20 M. Röttger, T. Domenech, R. van der Weegen, A. Breuillac, R. Nicolaÿ, L. Leibler, *Science* **2017**, 356, 62.

21 N. J. Van Zee, R. Nicolaÿ, *Prog. Polym. Sci.* **2020**, 104, 101233.

22 D. Demongeot, R. Groote, H. Goossens, T. Hoeks, F. Tournilhac, L. Leibler, *Macromolecules* **2017**, 50, 6117.

23 L. Farge, S. Hoppe, V. Daujat, F. Tournilhac, S. André, S., *Macromolecules* ***2021***, 54, 1838.

24 C. G'sell, N.A. Aly-Helal, J.J.Jonas, *J. Mater. Sci* **1983**, 18, 1731.

25 C. G'sell, J.J.Jonas, *J. Mater. Sci* **1979**, 14, 583.

26 H.G.H. Van Melick, L.E. Govaert, H.E.H Meijer, *Polymer* **2003**, 44, 2493.

27 L.C. Van Breemen, T.A. Engels, E.T. Klompen, D.J. Senden, L.E. Govaert, *J. Polym. Sci. B: Polym. Phys.* **2012**, 50, 1757.

28 R.N. Haward, *Macromolecules* **1993**, *26*, 5860.

29 W. Zhang, J. Li, H. Li, S. Jiang, S., L. An, Polymer **2018**, 143, 309.

30 T. B. Van Erp, C. T. Reynolds, T. Peijs, J. A. Van Dommelen, L. E. Govaert, *J. Polym. Sci. B: Polym. Phys.* **2009**, 47, 2026.

31 D. Zhou, S.G. Yang, J. Lei, B.S. Hsiao, Z.M. Li, *Macromolecules* **2015**, 48, 6652.

32 R.H. Somani, L. Yang, L. Zhu, B.S. Hsiao, *Polymer* **2005**, 46,8623.

33 E.L. Heeley, T. Gough, D.J. Hughes, W. Bras, J. Rieger, A.J. Ryan, Polymer 2013, 54, 6580.

34 D. Mi, M. Zhou, F. Hou, J. Zhang, *J. Appl. Polym. Sci.* **2018**, 135, 46465.

Acknowledgements

The authors would like to thank the ICEEL Carnot Institute, the EMPP research department of Lorraine University, the Grand Est Region and ADEME (french agency for ecological transition) for their financial support. We are also very grateful to Jérémy Bianchin who made the injection specimen mold.

Supporting Information

Development of plasticity in vitrimers synthesized from a semi-crystalline polymer using Injection Molding

L. Farge[1*], R. Spiegel[1], S. André[1], C. Noûs[1,3], R. Lainé[2], S.Hoppe[2]

1 Université de Lorraine, CNRS, LEMTA, F-54000 Nancy, France

2 Université de Lorraine, CNRS, LRGP, F-54000 Nancy, France

3 Cogitamus Laboratory, F-75005 Paris, France.

*Corresponding author: laurent.farge@univ-lorraine.fr

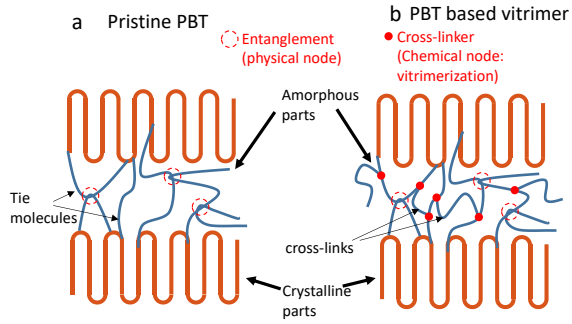

Figure S1 Schematic representation of the pristine PBT (a) and vitrimer (b) microstructures.

Figure S2 Specimen mold.

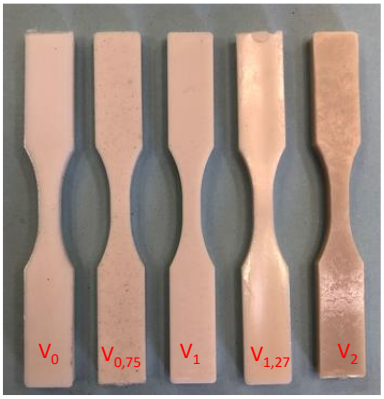

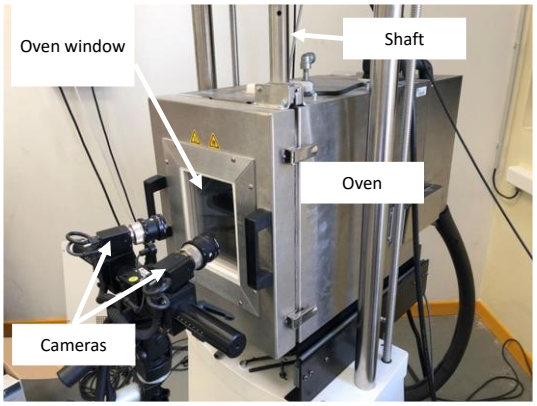

Figure S3 Colour of specimens.

Figure S4 Photography of the experimental set up.

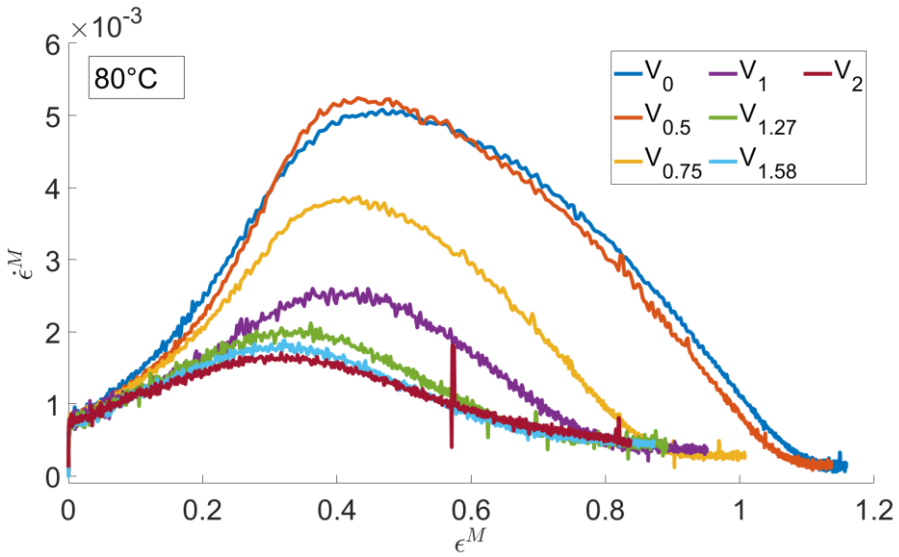

Figure S5 Strain rates in the neck center $\dot{\varepsilon}^M$ versus ε^M at 80°C.

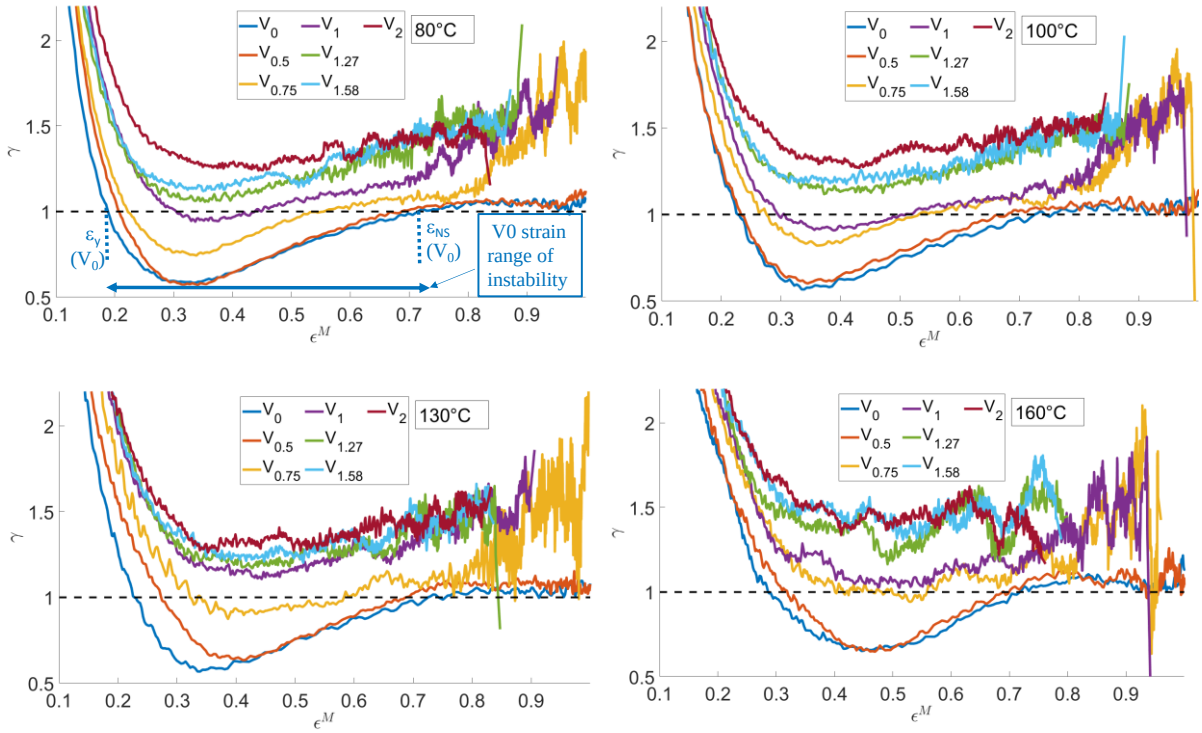

Figure S6 Strain-hardening coefficient $\gamma\left(\varepsilon^M\right)=\frac{\ln\sigma}{d\varepsilon^M}$ *versus* ε^M *at the four temperatures.*

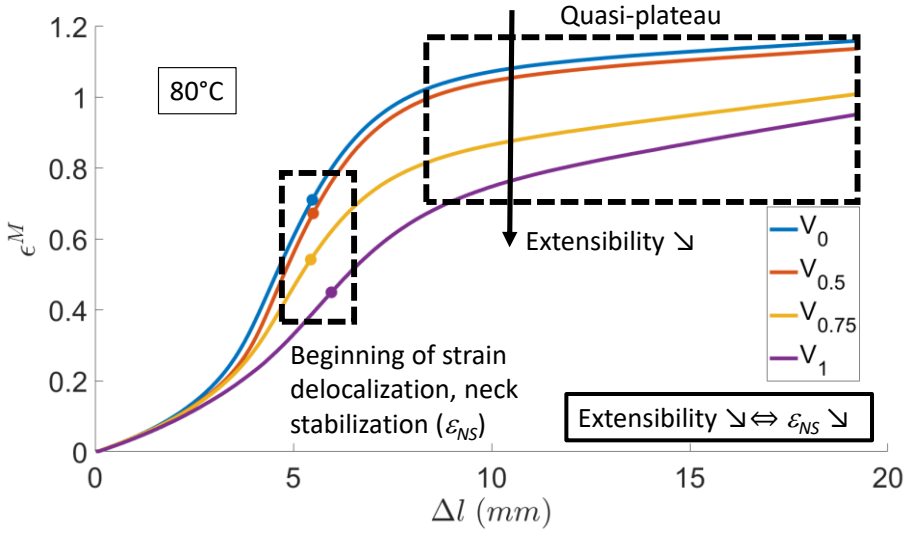

Figure S7 ε^M *versus* Δl *(crosshead relative displacement) at 80°C for* V_0, $V_{0.5}$, $V_{0.75}$ *and* V_1 *(YPTC behavior). This illustration is intended to show that it is possible to compare the limitation in extensibility of different polymers through the measurement of* ε_{NS}.

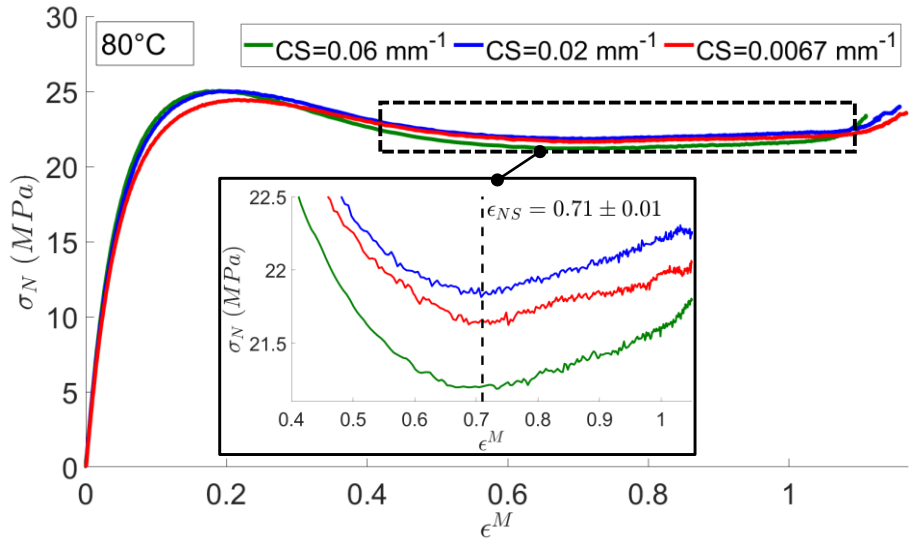

Figure S8 Influence of the strain rate on ε_{NS}*:* σ_N *versus* ε^M *at three different Crosshead Speeds (CS) at 80°C for* V_0*. The inset is an enlargement of the zone (*σ_N *minimum) where* ε_{NS} *is measured.*

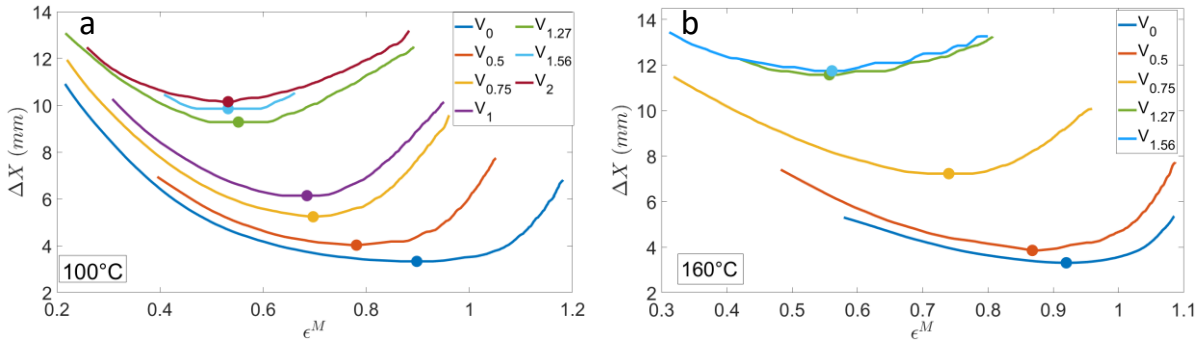

Figure S9 Evolutions of ΔX against ε^M at 100°C (a) and 160°C (b). In the latter case, the V_1 and V^2 curves cannot be shown because the 3 D DIC software only managed to compute strains in a small interval around the specimen center.